

# Seminar Spring '10

# *Three-Dimensional Inverse Scattering of a Dielectric Target Embedded in a Lossy Half-Space*

*Yijun Yu, Tiejun Yu, Senior Member, IEEE, and Lawrence Carin, Fellow, IEEE*  
(IEEE TRANSACTIONS ON GEOSCIENCE AND REMOTE SENSING, VOL. 42, NO. 5, MAY 2004)

# Claim to Fame

- Early work in inverse scattering(Born and Rytov approximation, iterative Born, DBIM and modified gradient) had been carried out in 2-D space mostly assuming a homogeneous background medium.
- The authors believe that this paper represents one of the first complete 3-D inversions of sub-sensing data.

# Abstract

- Modified **iterative Born method** for 3-D inversion of a lossless dielectric target embedded in a lossy half-space.
- The **forward solver** employs a modified form of the extended Born method, and the half-space Green's function is computed efficiently via the **complex-image technique**.
- Simple **Tikhonov regularization** is employed which yields adequate results for inversion of noisy data.

# Introduction

- **Motivation:** Imaging of buried plastic land mines
- Consideration of half-space or layered medium background escalates the computational complexity of the inversion significantly, due to the need to compute the dyadic background Green's function and also the sensors are incompatible with a 2-D approximation.
- In this paper imaging of dielectric targets embedded in a lossy half-space, at radar frequencies (example results are presented for sensing at 500 MHz) is considered.
- Loop antenna is used as Tx and separate bistatic loops as Rx.
- Scattered-field data is obtained via MoM, same forward solver is used for inversion but distinct meshes are used to avoid an 'inverse crime'. Fields are computed via extended Born Method.
- Zero mean AWGN added results are also shown.

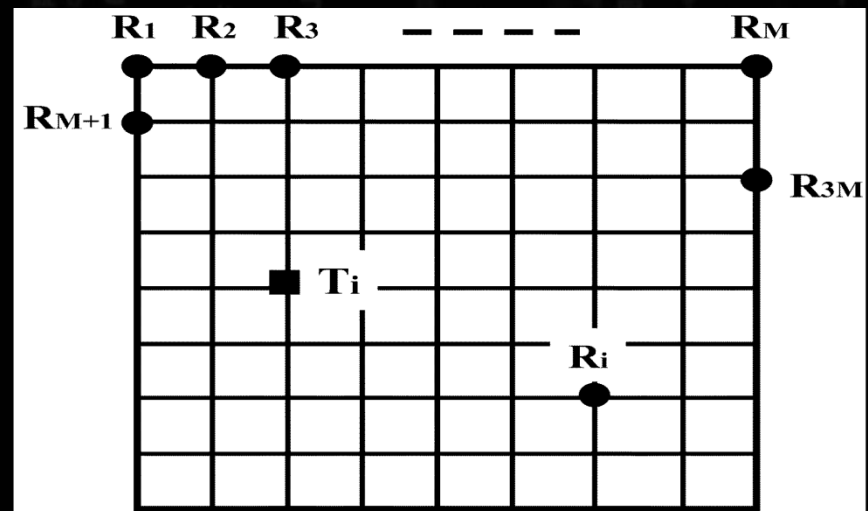
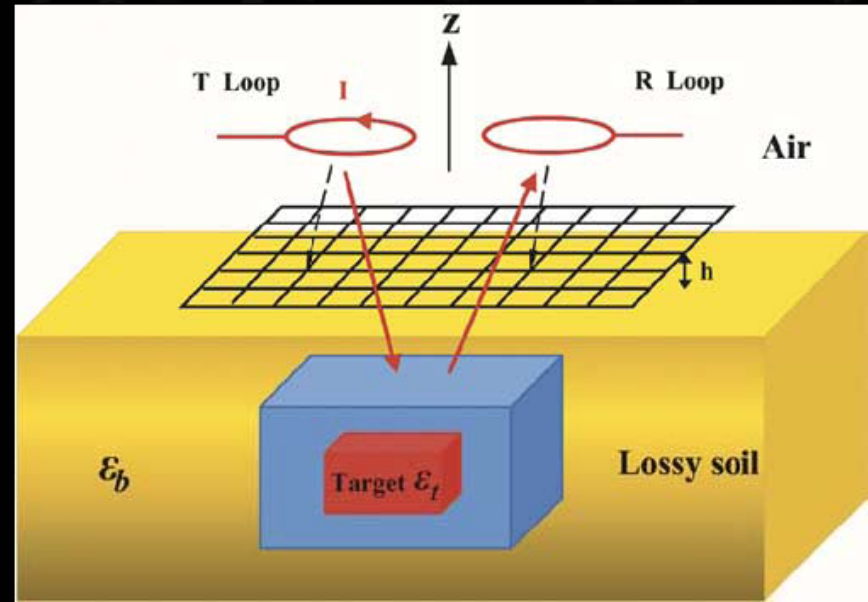
# Sections

- Forward Models
- 3-D inversion Schemes
- Example Results

# FORWARD MODELS

## A. Problem Statement:

A loop antenna is used as the sensor under consideration, with a second set of (bistatic) loops used for reception (see Fig. 2). The target of interest is buried in a homogeneous lossy dielectric half-space (Fig. 1). The objective is inversion for the target shape and its electrical properties. Multiple ( $M^4$ ) bistatic measurements are taken just above the air-ground interface, and operation is considered at a single frequency, although multiple frequencies are likely to provide additional information and improved inversion performance.



## B. Reference Scattered Fields:

- In inversion measured scattered fields at various sensor positions is required which in this modeling has been computed using MoM in which half space dyadic Green's Function being computed via the CIT(which too has its limitations below 50MHz and in case of partially buried objects or multilayered modeling of background medium).
- But since for the extended Born, the interactions b/w source and observer are calculated in the subsurface so CIT will work efficiently.
- In cases where CIT fails the space domain Dyadic Green's function is put in pre-computed LUT's(e.g. in Window-based acceleration technique).

## C. Electric Fields inside targets:

Assuming the excitation loop current parallel to the air-ground interface  $I$  to be known and uniformly distributed about the transmitter coil, the incident field in the sub-surface is given as:

$$\mathbf{E}^{\text{inc}}(\mathbf{r}) = I \oint_C \mathbf{G}_{\text{EJ}} \cdot d\mathbf{l} = I \int_{\Delta S} (\mathbf{x} \sin \theta - \mathbf{y} \cos \theta) G_{\text{EH}} ds$$

where  $\Delta S$  is the surface area of the loop and  $\theta$  is the angle b/w projection of  $\mathbf{r}-\mathbf{r}'$  on x-y plane and x-axis while  $G_{\text{EH}}$  is defined as:

$$\begin{aligned} G_{\text{EH}} &= S_1[\tilde{G}_{\text{EH}}] \\ \tilde{G}_{\text{EH}} &= \frac{1}{2\pi\omega\epsilon_0} \frac{k_{z1} - k_{z0}}{\epsilon_r - 1} \exp[-jk_{z0}z' + jk_{z1}z] \\ S_n[\tilde{G}(k_\rho)] &= \int_0^\infty \tilde{G}(k_\rho) J_n(k_\rho \rho) k_\rho^{n+1} dk_\rho. \end{aligned}$$

where

$$k_{z1} = [k_1^2 - k_\rho^2]^{1/2} \text{ and } k_{z0} = [k_0^2 - k_\rho^2]^{1/2}$$

$k_0$  and  $k_1$  are the wavenumbers of air and soil respectively.

- Assume that  $E(r)$  represents the electric field at position  $r$ . Using  $G_{EJ}$  to denote the component of the dyadic half-space Green's function representing induced electric fields in terms of excitation electric currents, we have

$$E(\mathbf{r}) = E^{\text{inc}}(\mathbf{r}) + j\omega \int_V [\varepsilon_t(\mathbf{r}') - \varepsilon_b(\mathbf{r}')] G_{EJ}(\mathbf{r}, \mathbf{r}') \cdot E(\mathbf{r}') d^3\mathbf{r}'$$

- Since  $G_{EJ}$  is large for  $r$  in the vicinity of  $r'$ , while being relatively small for  $r$  distant from  $r'$ :

$$E(\mathbf{r}) \approx E^{\text{inc}}(\mathbf{r}) + j\omega \int_V [\varepsilon_t(\mathbf{r}') - \varepsilon_b(\mathbf{r}')] \cdot G_{EJ}(\mathbf{r}, \mathbf{r}') E(\mathbf{r}') d^3\mathbf{r}', \quad \mathbf{r} \in V$$

which can be rearranged to get :

$$E(\mathbf{r}) \approx M(\mathbf{r})^{-1} \cdot E^{\text{inc}}(\mathbf{r}), \quad \mathbf{r} \in V$$

$$M(\mathbf{r}) \equiv I - j\omega \int_V G_{EJ}(\mathbf{r}, \mathbf{r}') [\varepsilon_t(\mathbf{r}') - \varepsilon_b(\mathbf{r}')] d^3\mathbf{r}'$$

now this gives approximate  $E(r)$  inside the target which can be used in the above exact formula to find field everywhere.

- In classical Born Approximation the integral term is missing while for extended Born approximation  $\varepsilon_t(r) - \varepsilon_b(r)$  are represented as a piece-wise constant scalar function of  $N$  3-D cubes.

- Then  $\mathbf{M}(\mathbf{r})$  is computed at  $N$  centers of the cubes so that  $\mathbf{E}$  is expressed as

$$\mathbf{E}(\mathbf{r}_n) = \mathbf{M}(\mathbf{r}_n)^{-1} \cdot \mathbf{E}^{\text{inc}}(\mathbf{r}_n) \quad \text{where} \quad \mathbf{M}(\mathbf{r}_n) \equiv \mathbf{I} - j\omega\epsilon_b \sum_{k=1}^N a_k \mathbf{G}_k(\mathbf{r}_n)$$

$$\mathbf{G}_k(\mathbf{r}_n) = \int_{V_k} \mathbf{G}_{\text{EJ}}(\mathbf{r}_n, \mathbf{r}') d^3\mathbf{r}'$$

- So Extended Born Method requires inversion of  $N$  3x3 matrices, thus  $O(N)$  complexity, but computation of  $N$   $\mathbf{M}(\mathbf{r})$  also requires  $O(N^2)$  driven by  $N^2 \mathbf{G}_k(\mathbf{r}_n)$ . Thus the computation of  $\mathbf{E}(\mathbf{r})$  is still expensive. Thus further approximating by only including the near cube interactions  $\mathbf{G}_n(\mathbf{r}_n)$  to compute the integral.

## D. Efficient Computation of the Scattered Field:

From the fields inside the target obtained via extended Born method we can write:  $\mathbf{J}(\mathbf{r}) = j\omega[\epsilon_t(\mathbf{r}) - \epsilon_b(\mathbf{r})]\mathbf{E}(\mathbf{r})$  whereas the voltage measured in a small receiver coil at  $\mathbf{r}_s$  is

$$V(\mathbf{r}_s) = -j\omega\mu_o\Delta S \mathbf{z} \cdot \int_V \mathbf{G}_{\text{HJ}}(\mathbf{r}_s, \mathbf{r}') \cdot \mathbf{J}(\mathbf{r}') d^3\mathbf{r}'$$

$$= -\Delta S \int_V [\sin\theta J_x - \cos\theta J_y] G_{\text{HJ}} d^3\mathbf{r}'$$

$$G_{\text{HJ}} = S_1[\tilde{G}_{\text{HJ}}]$$

$$\tilde{G}_{\text{HJ}} = \frac{k_{z1} - k_{zo}}{2\pi\omega\epsilon_o(\epsilon_r - 1)} \exp(jk_{z1}z' - jk_{zo}z)$$

The above expression manifests the usual convolutional form inherent b/w sources and observation points so for each iteration FFT can be employed.

# Inversion Scheme

## A. Iterative Born:

The measured voltage can be written as:

$$\boldsymbol{v} = \boldsymbol{Z}\boldsymbol{a}$$

which itself is nonlinear in the profile  $\boldsymbol{a}$  as  $\boldsymbol{Z}$  is a function of  $E(r)$  in the subsurface being dependant on  $\boldsymbol{a}$ .

- An assumed  $\boldsymbol{a}_0$  is used as a starting point, for which  $\boldsymbol{E}$  then  $\boldsymbol{J}$  and ultimately  $\boldsymbol{Z}$  is calculated which is then used to calculate  $\boldsymbol{a}_1$  via:

$$\boldsymbol{a}_1 = \boldsymbol{Z}^+ \boldsymbol{v}$$

where  $\boldsymbol{Z}^+$  is the Moore-Penrose pseudo-inverse. The process is now repeated iteratively until  $\boldsymbol{a}_n$  converges.

- In each of the iterative Born inversion, the half space Green's function characteristic of the background half-space is used. This implies that the inhomogeneity contrast should be relatively small. If not then DBIM must be employed. But in this paper only half-space Green's function is utilized.

## B. Regularization:

- For the  $k^{\text{th}}$  iteration of the iterative Born Solution, the least square solution corresponds to finding the coefficients  $a_k$  that minimizes  $\|\mathbf{Za}_k - \mathbf{v}\|^2$  (2 norm is used) .
- Tikhonov regularization corresponds to finding the coefficients  $a_k^\alpha$  that minimizes  $\|\mathbf{Za}_k^\alpha - \mathbf{v}\|^2 + \alpha \|a_k^\alpha\|^2$  where  $\alpha > 0$  and according to authors the choice of the appropriate  $\alpha$  is often determined relatively quickly, but one must have *a priori* knowledge of the anticipated profile to assess the quality of  $a^\alpha$  .
- It is felt that there is significant room for improving the inversion algorithm itself, to avoid or minimize the importance of regularization parameters like  $\alpha$ .

## C. Parallel Algorithm Implementation:

- The simplified MPI implementation is a consequence of the fact that many of the computations required for inversion may naturally be implemented in parallel like Green's function's LUT and extended Born computation of fields within the target(which are independent for each cell).

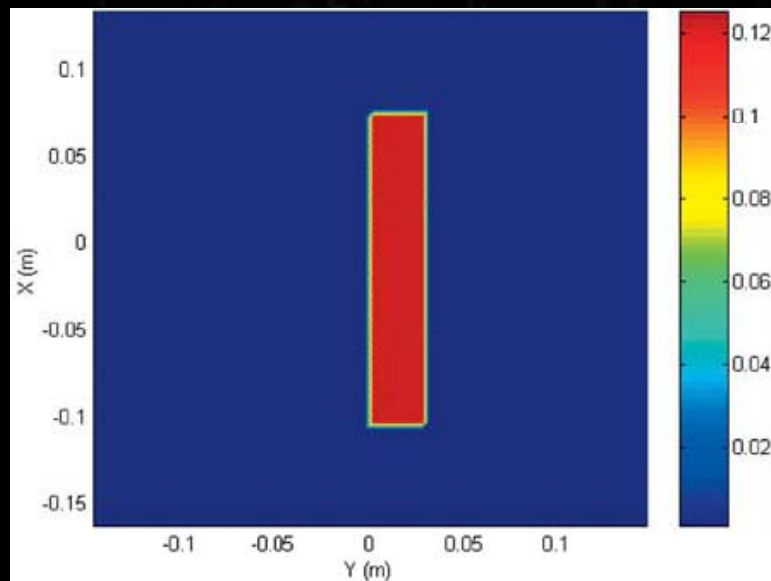
# Example Results

## A. Forward Models:

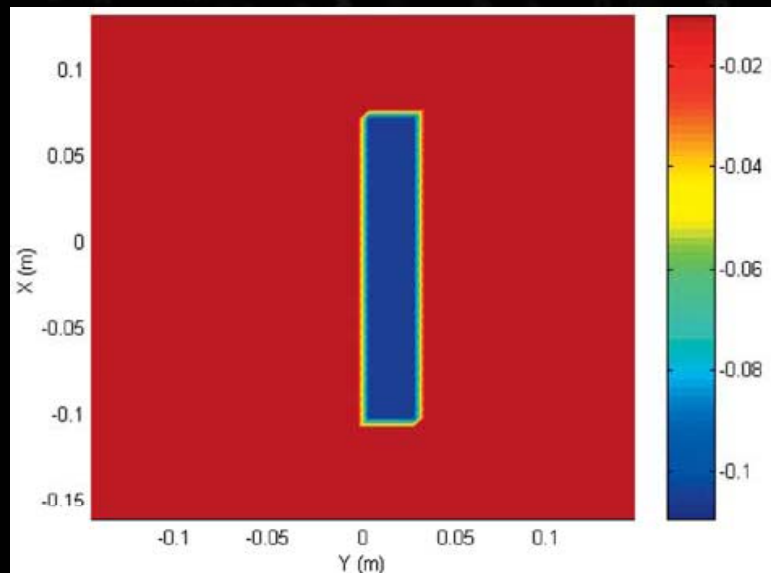
The following three models have been considered :

- 1) MoM
- 2) Extended Born Method
- 3) Modified Extended Born Method

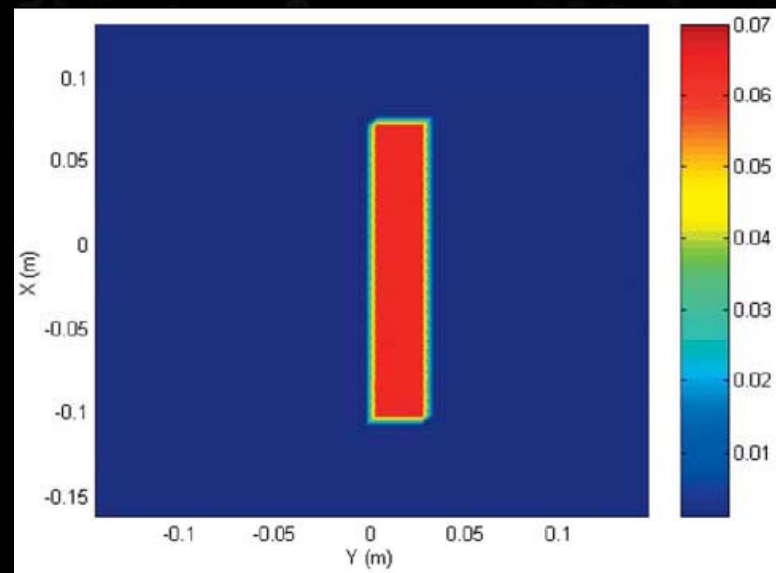
In this comparison the  $T_x$  loop antenna has a radius of  $r_t = 0.5\text{cm}$  and total current of 100A. The receiver loop has radius  $r_r = 0.5\text{cm}$ . The soil is modeled with  $\epsilon_r = 5 - j0.2$  and conductivity of  $\sigma = 0.01\text{ S/m}$ . The target is a dielectric box of lossless permittivity  $\epsilon_r = 4.5$ , dimensions 18cm x 3cm x 3cm, with target center buried at (0,0,-21.5cm), with computations performed at 500MHz.



**Magnitude**



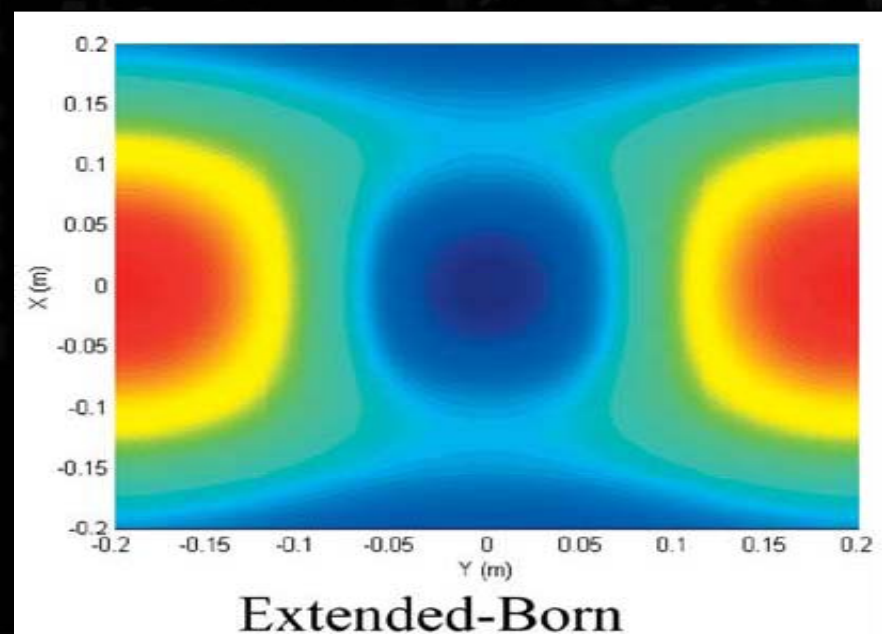
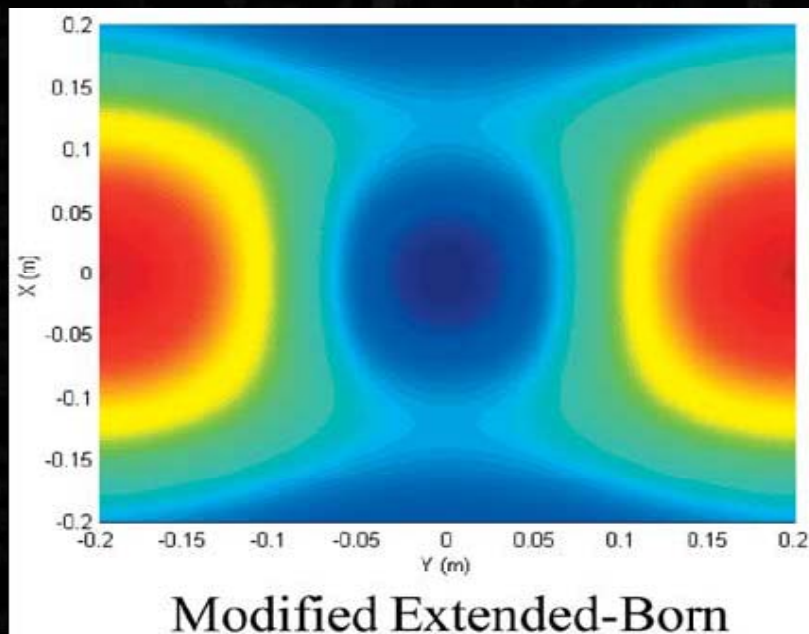
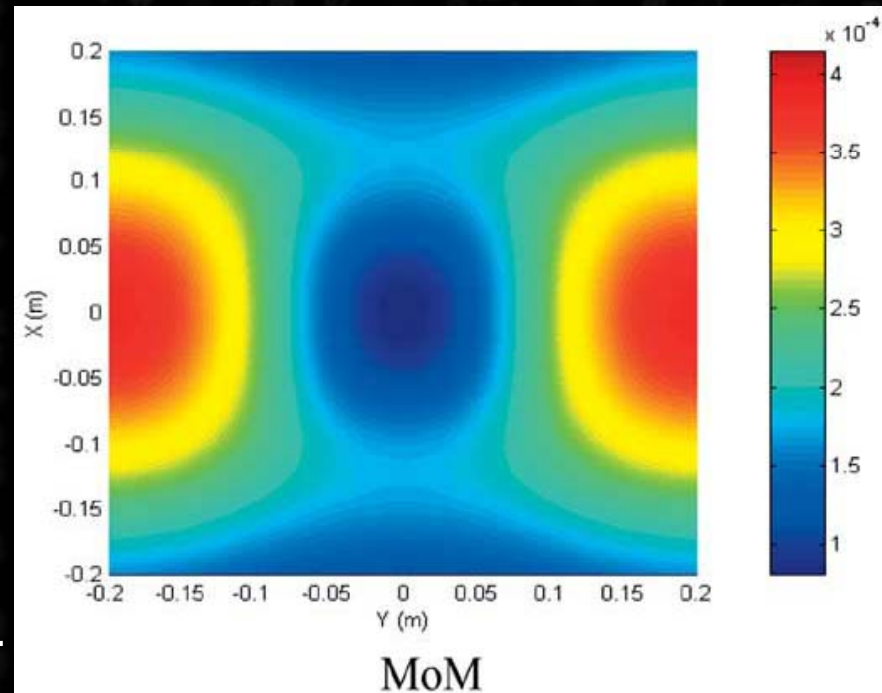
**Real Part**



**Imaginary Part**

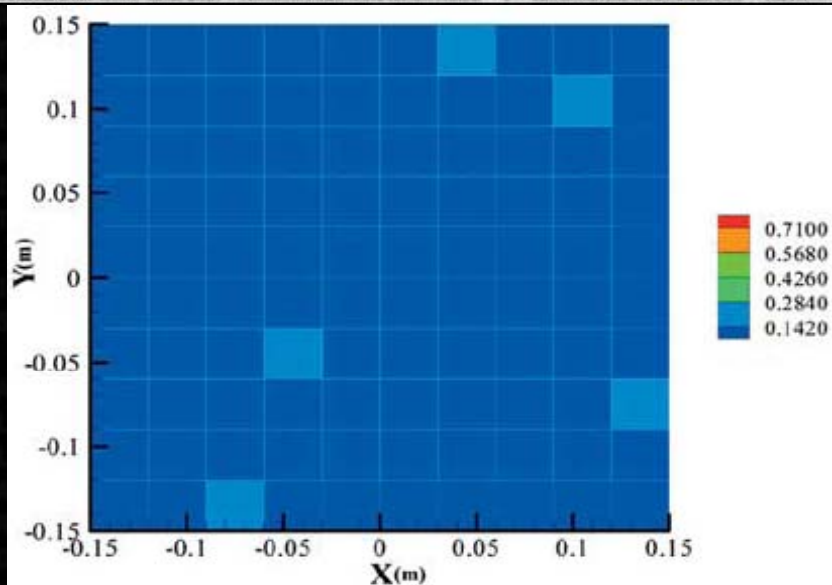
Cross section of a subsurface target, showing the magnitude of the contrast (top), the real part (left) and the imaginary part (right).

Scattered field results from the three models show that the simple modified extended Born Solution yields good results(at 500MHz). But as frequency decreases(e.g. to 100MHz),contrast increases (due to  $\sigma/\omega\epsilon$  term) and thus vitiating the simplest (self-term based) modified extended Born Method. Thus in all cases relatively weak contrast is considered; for higher contrast full extended Born method can be employed.

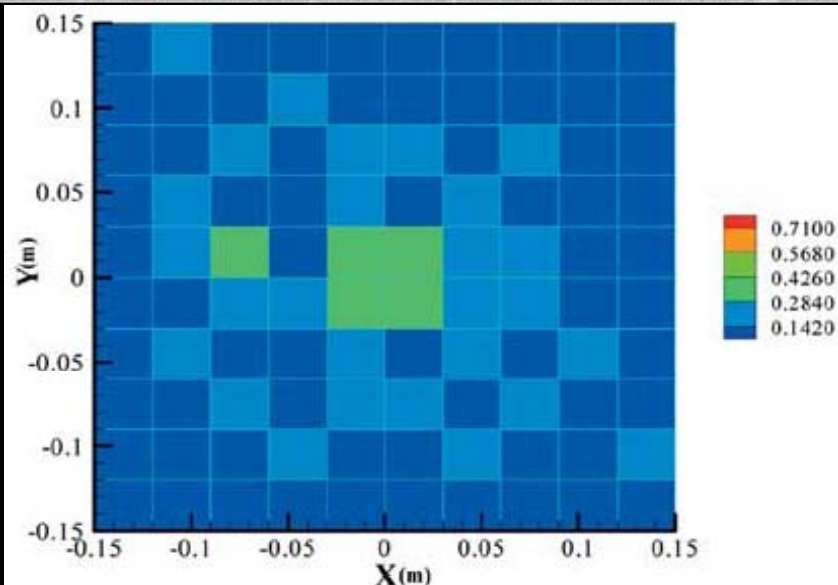


## B. Small-target High-contrast Inversion Example:

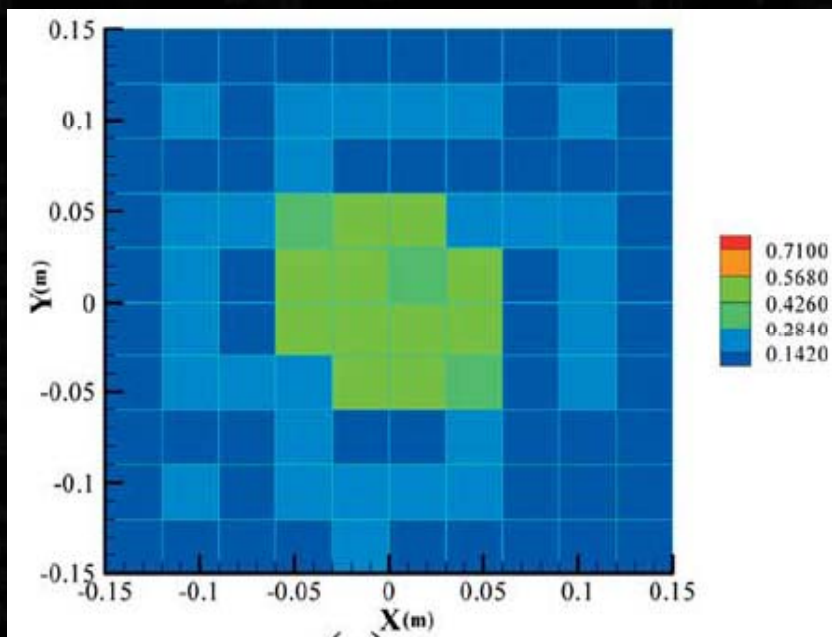
- Here, ten contiguous cube layers (with depth) are considered, each layer employing 10x10 cubes, for a total of 1000 complex unknowns.
- For computation of the “measured” scattered fields (to be inverted), via the volumetric MoM solution, the mesh cubic mesh is 4.1 cm on a side . In this forward computation, the target is composed of 3x3x3 cubes, encompassing 12.3 cm x12.3 cm x12.3 cm.
- The center of this target is situated in the center of the 10 x10 x 10 computational domain to be inverted, at a depth of 20 cm. In the inversion, each cube is 3 cm on a side. The true target position, therefore, encompasses 4x4x4 cubes in the center of the inversion domain, plus a *fraction of the true* target resides on the first set of cubes on the perimeter of these 64 cubes.
- $\epsilon_{rb} = 5 - j0.2$  and conductivity of soil  $\sigma = 0.01$  S/m .
- The target is a dielectric box of lossless permittivity  $\epsilon_{rt} = 1.0$ .
- Actual contrast  $a_n = -0.8 + j0.2$  (i.e.  $|a_n| = 0.8$ )
- Plots for only AWGN with Std. deviation of 5% are shown. (SNR=23dB)



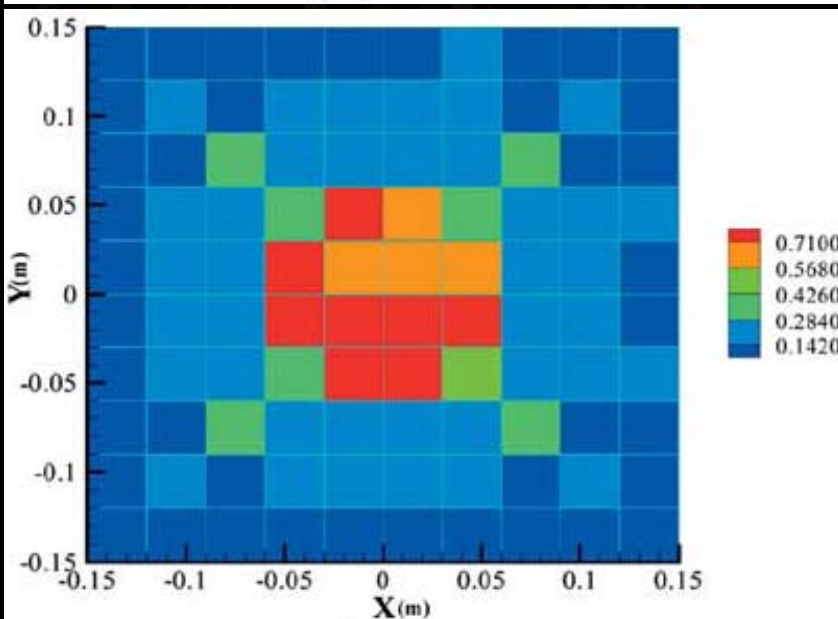
(a)



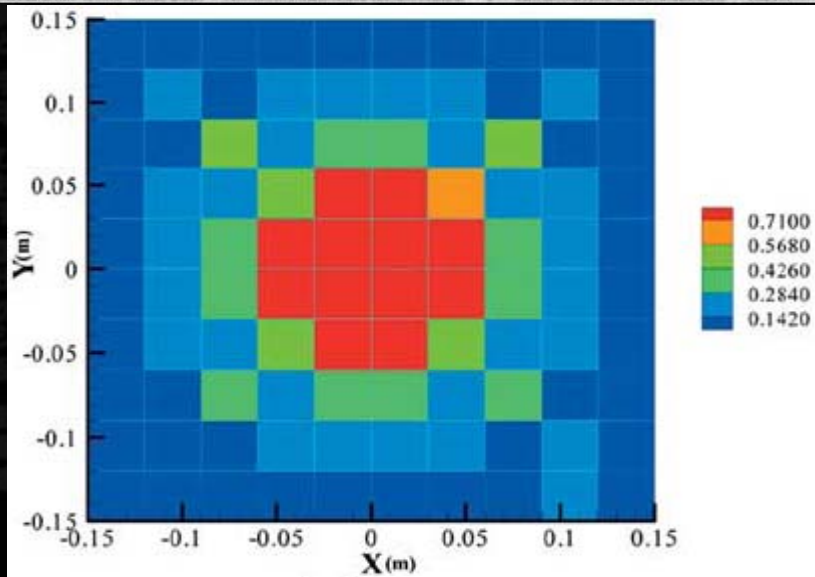
(b)



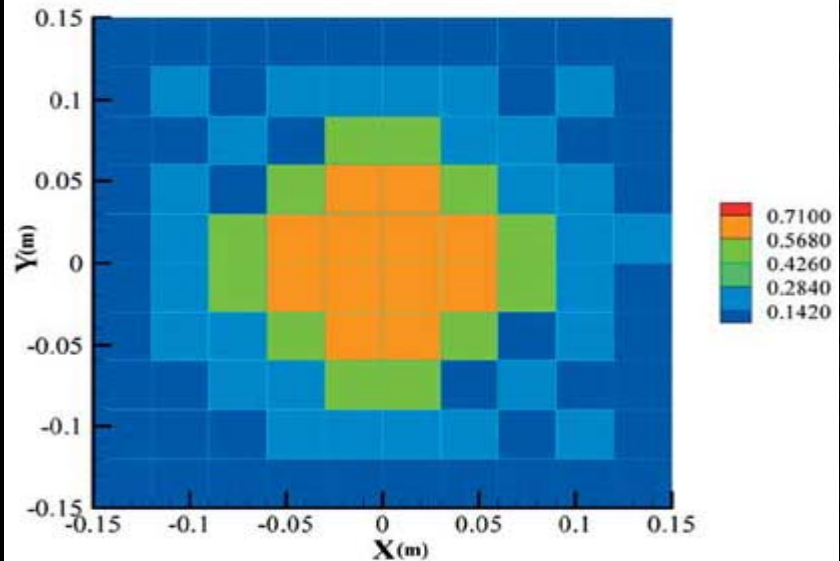
(c)



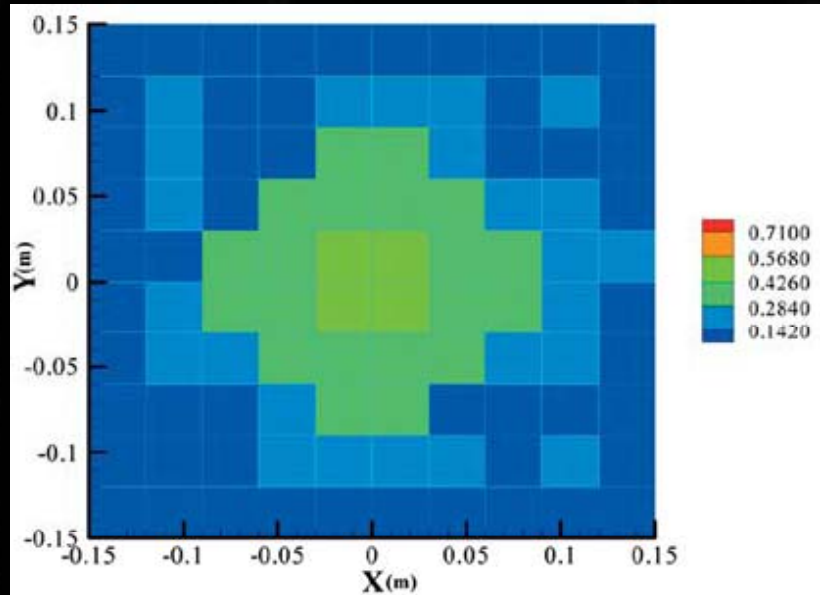
(d)



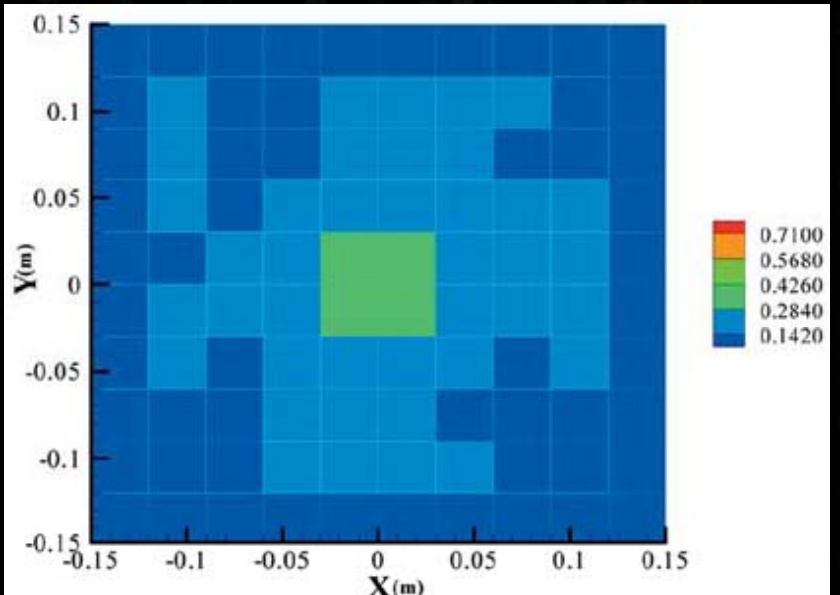
(e)



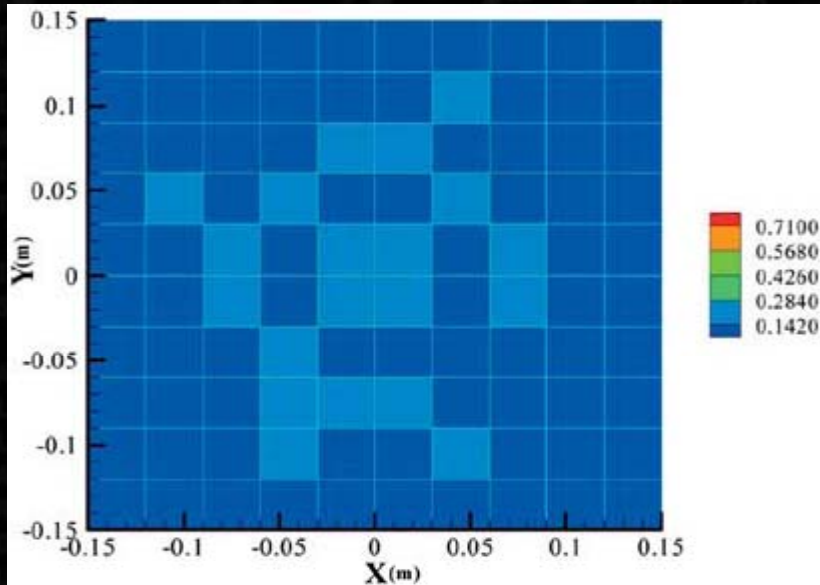
(f)



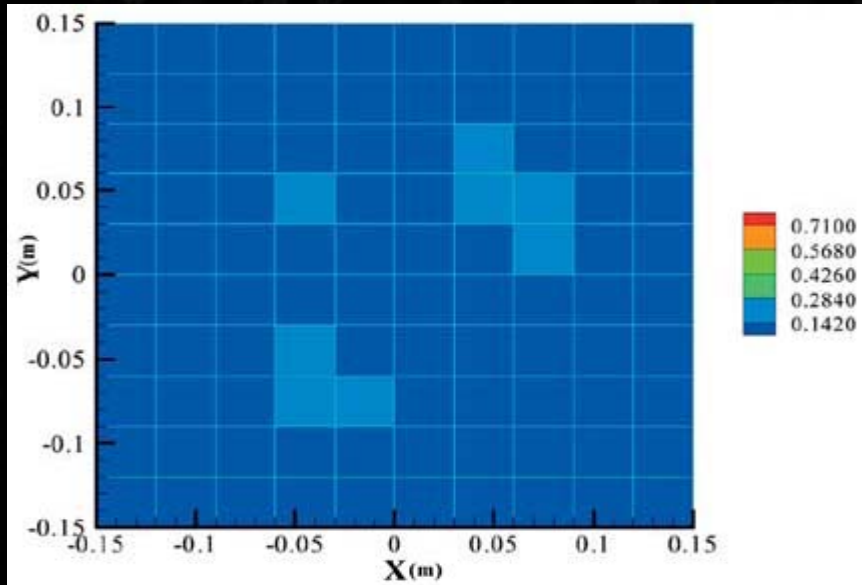
(g)



(h)

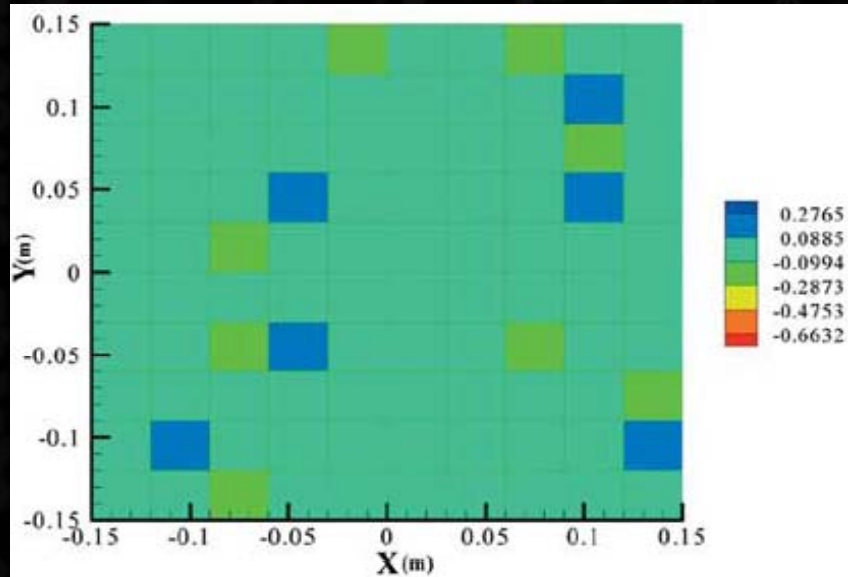


(i)

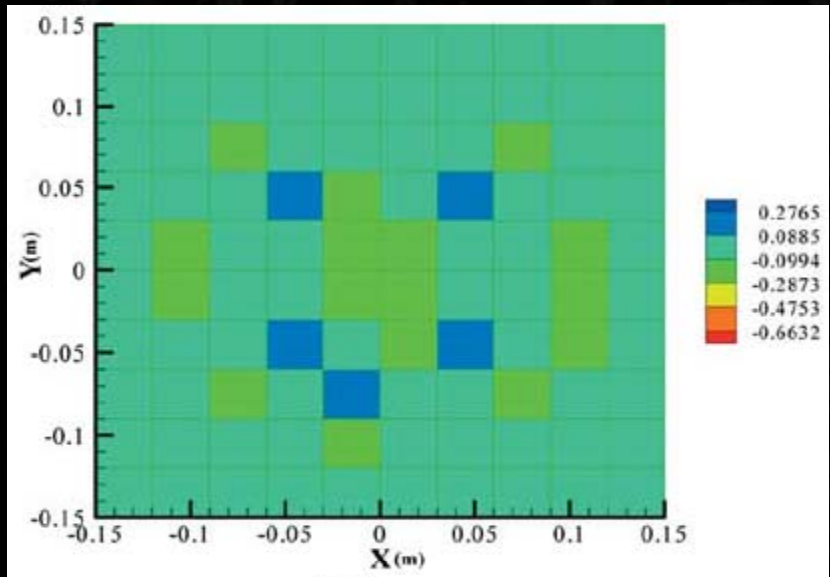


(j)

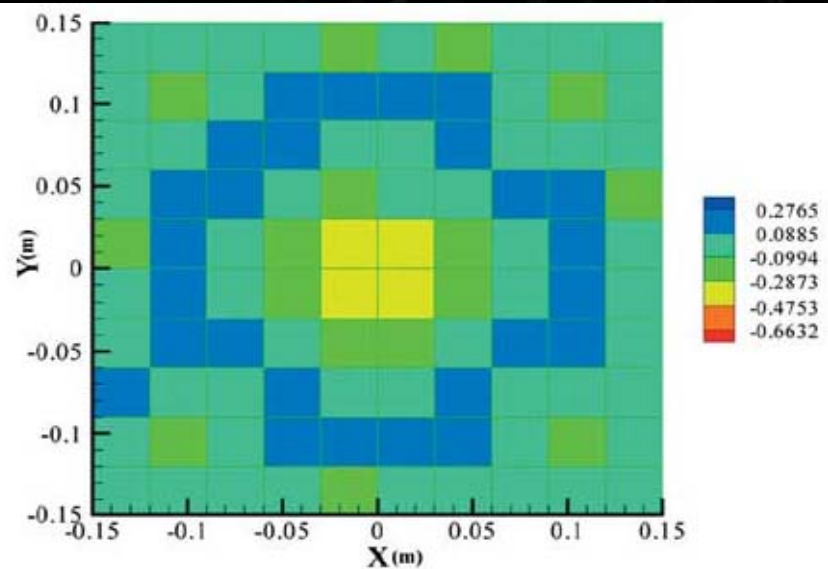
- Ideally in layer 5-8 the contrast should be close to true value of  $|a_n|=0.8$  as the object is situated here but in layers 4-7 the average contrast is  $|a_n|=0.59$  showing an error of 26%. Here Tikhonov parameter is set to  $1 \times 10^{-4}$ .
- In the forth coming figures the real and imaginary parts are plotted again in those the target can easily be distinguished in the middle 4 layers as it should be. The variation again is due to large contrast.



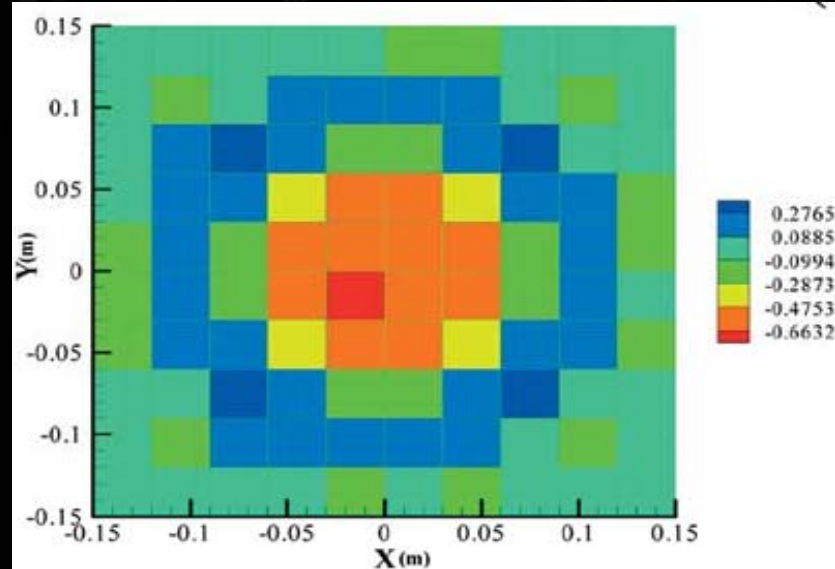
(a)



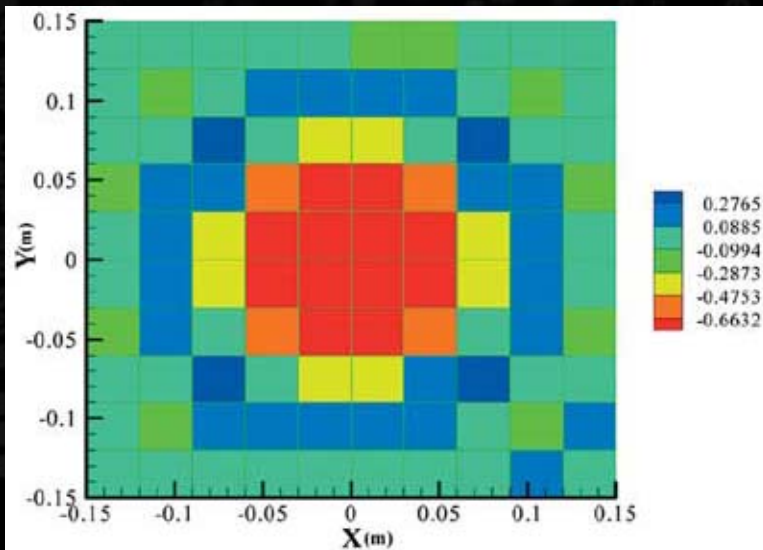
(b)



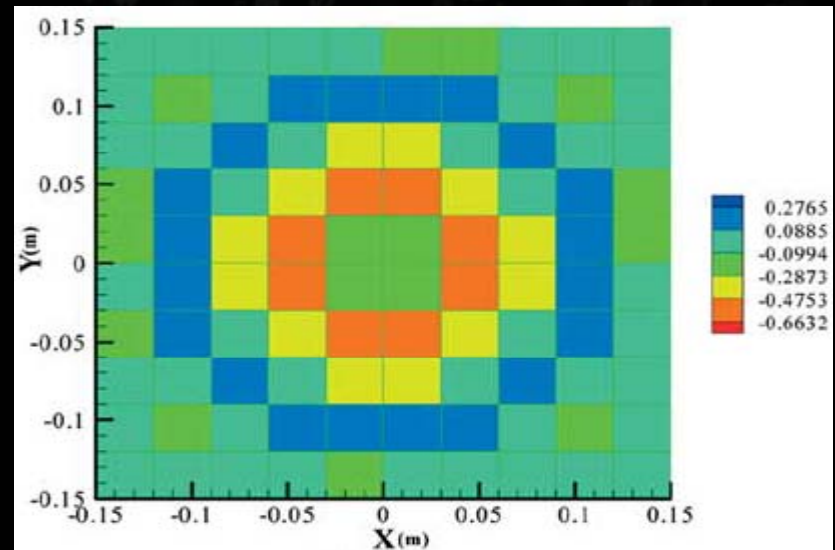
(c)



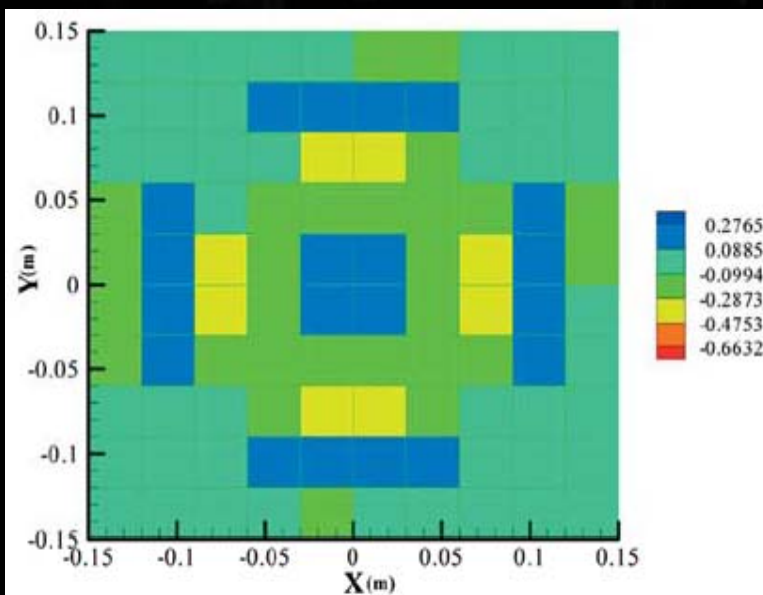
(d)



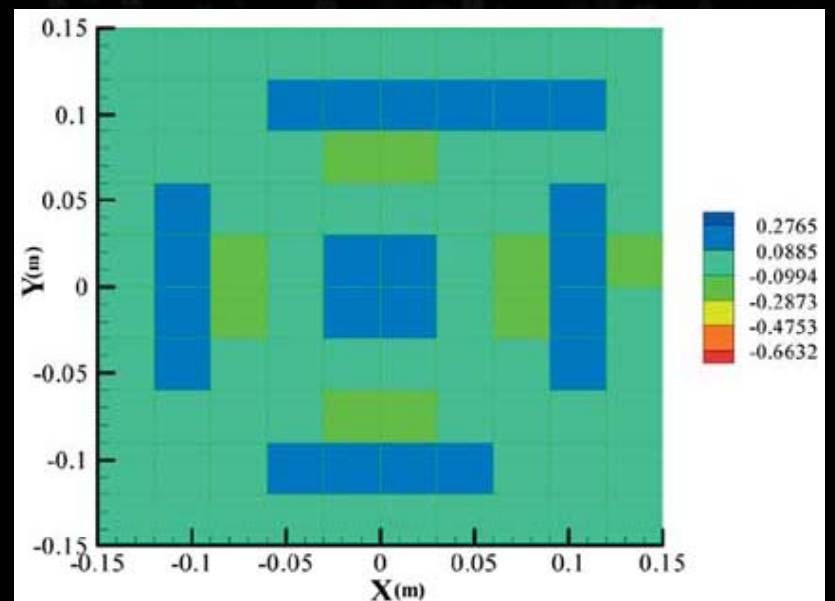
(e)



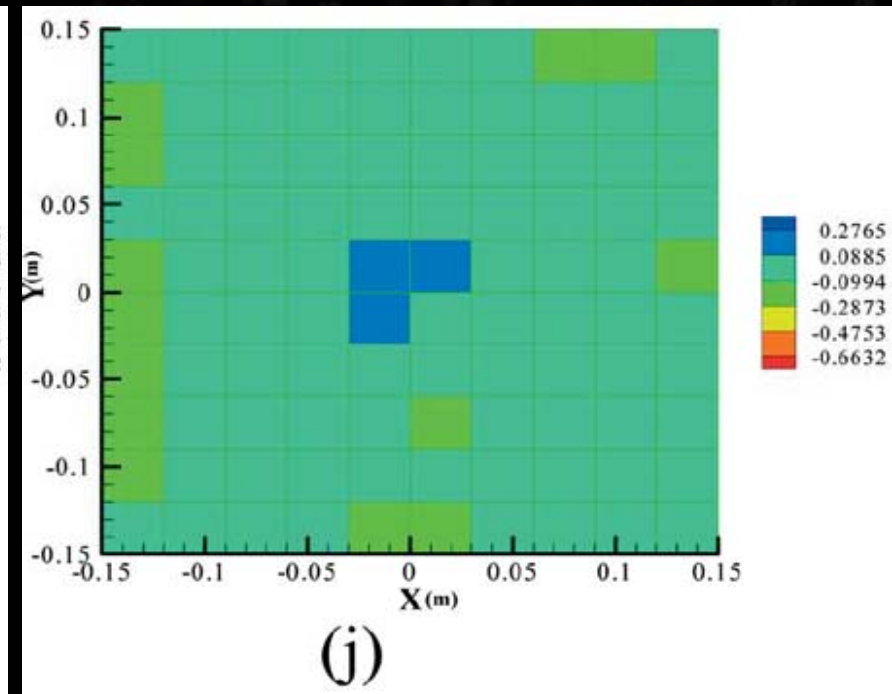
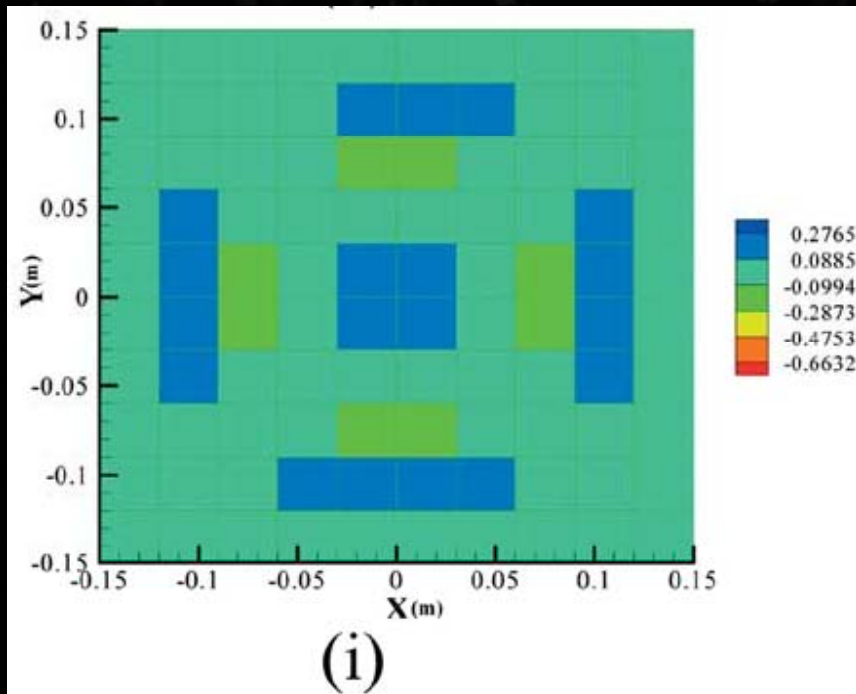
(f)



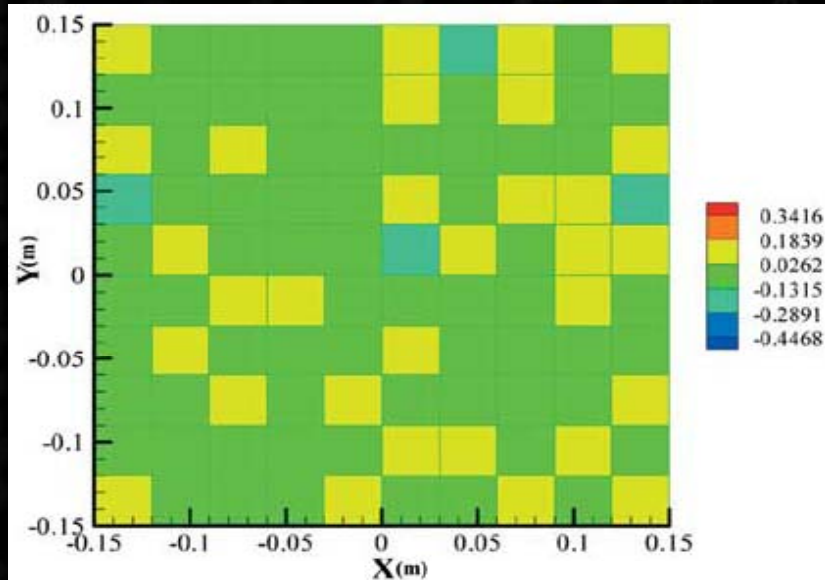
(g)



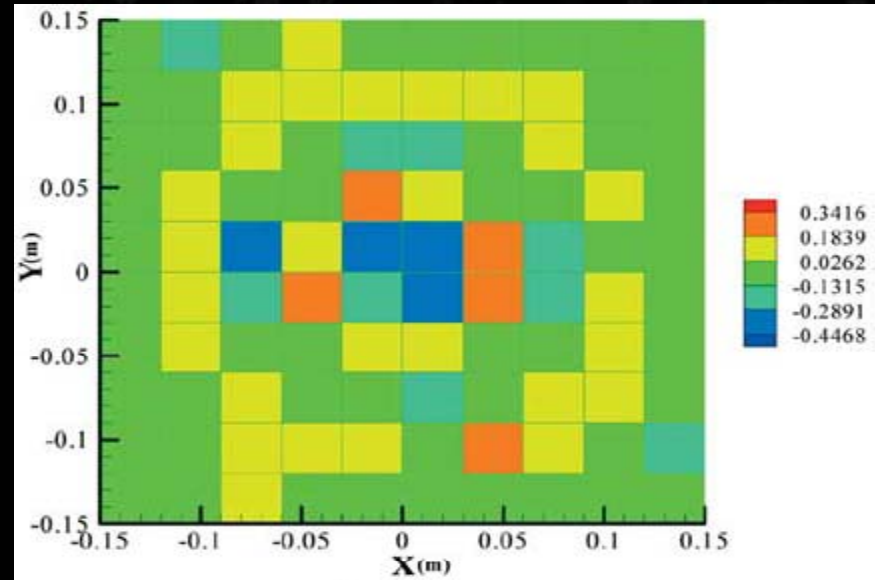
(h)



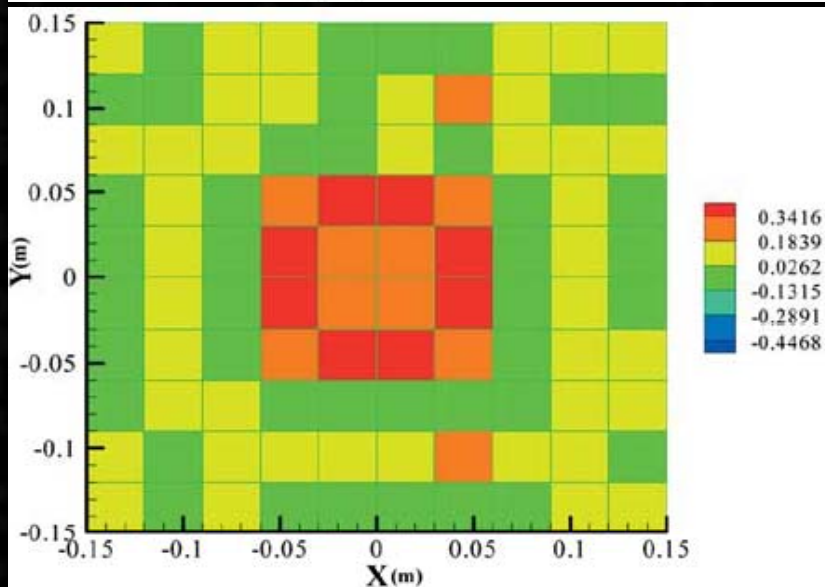
- Here from (a)-(j) the real part of the inversion was shown. Now the next 10 figures show the imaginary part.



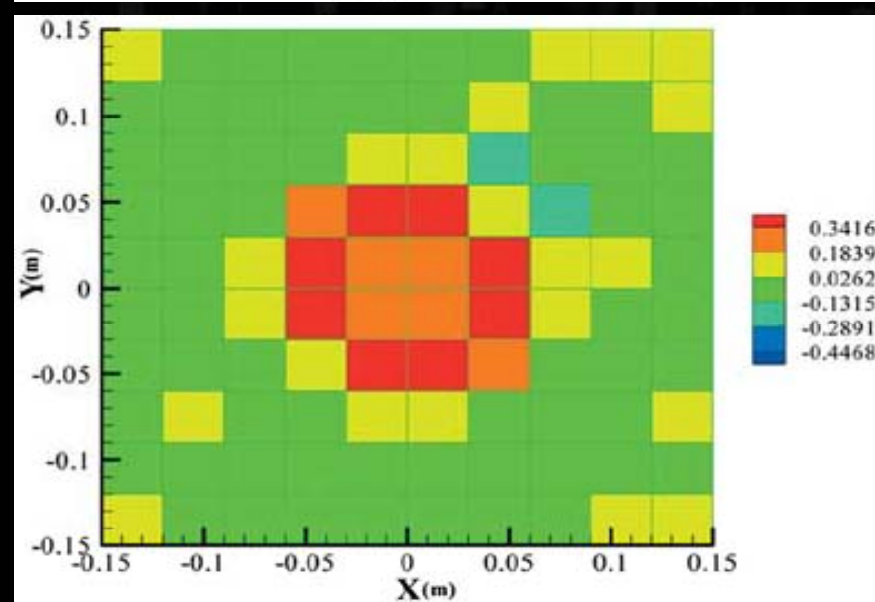
(a)



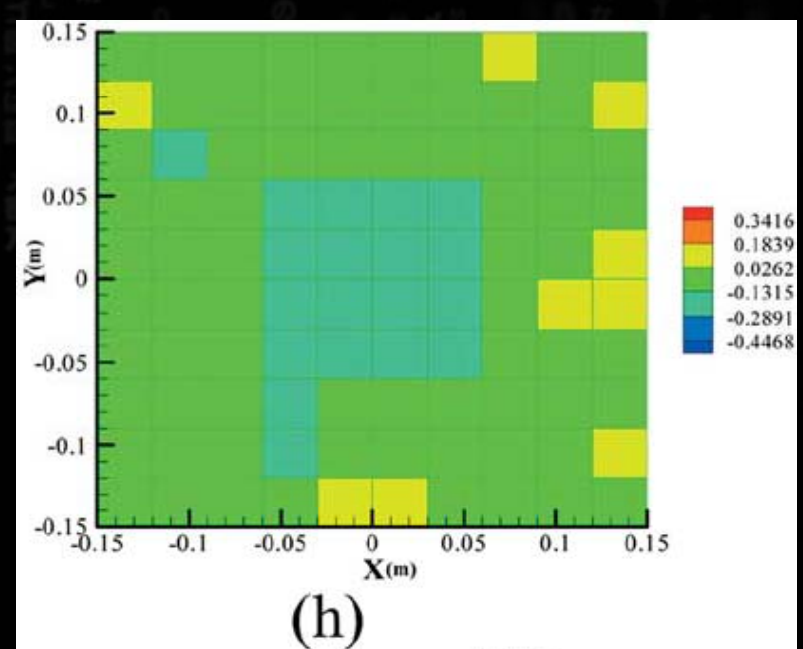
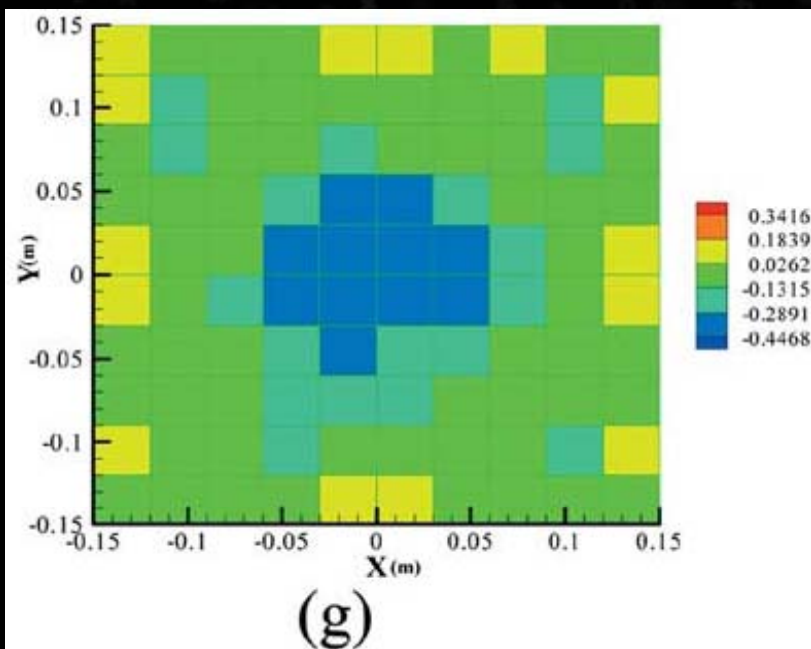
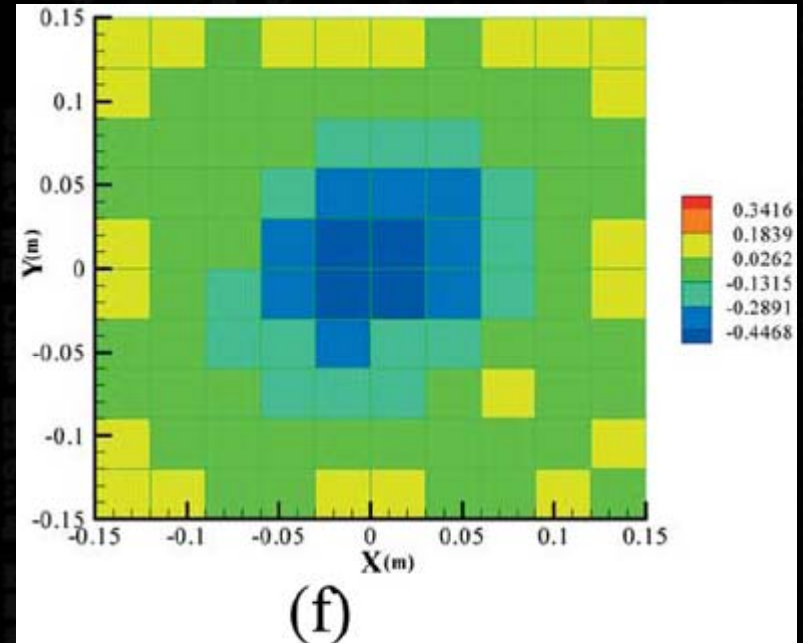
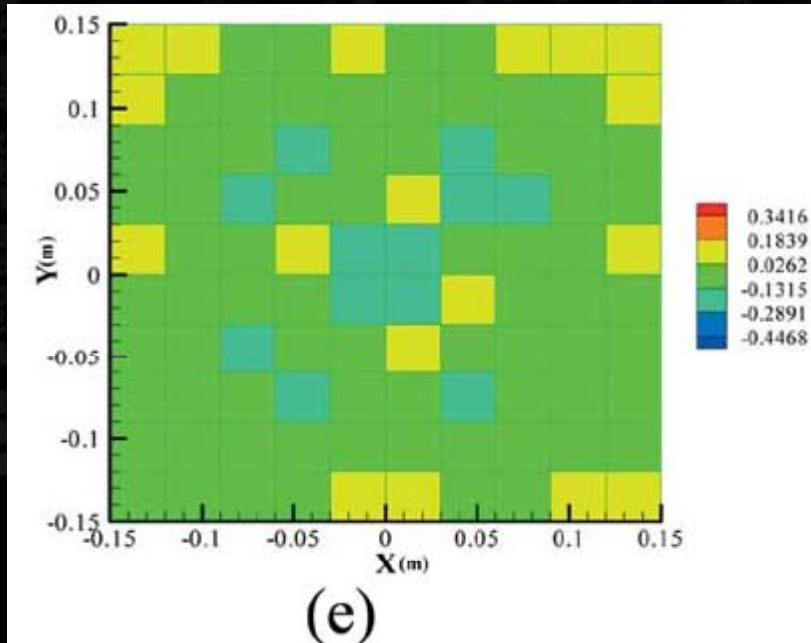
(b)

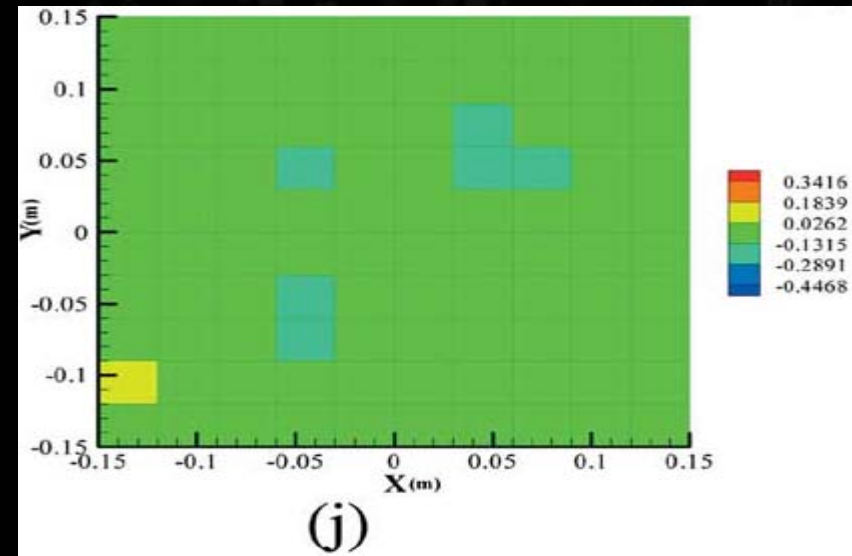
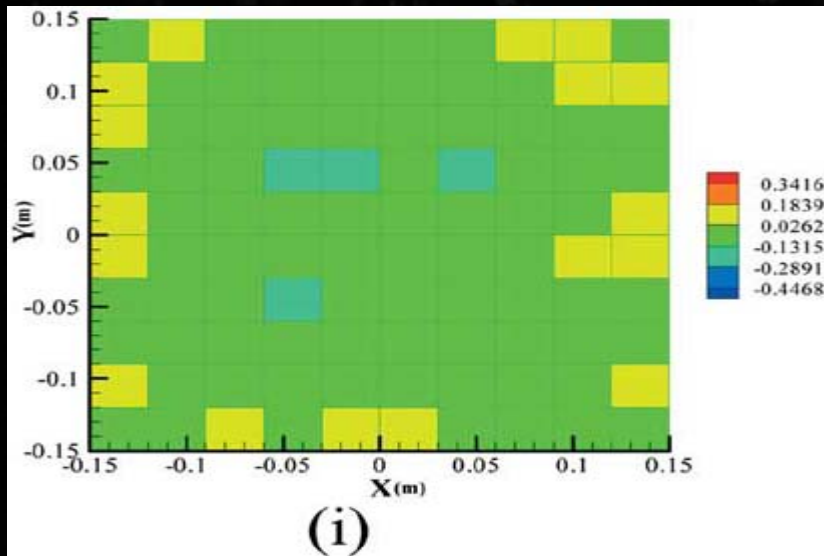


(c)



(d)





- The Convergence rate of the method as a function of number of iterations is plotted which shows that for this particular example the residual error falls well below 2% just after 5<sup>th</sup> iteration.

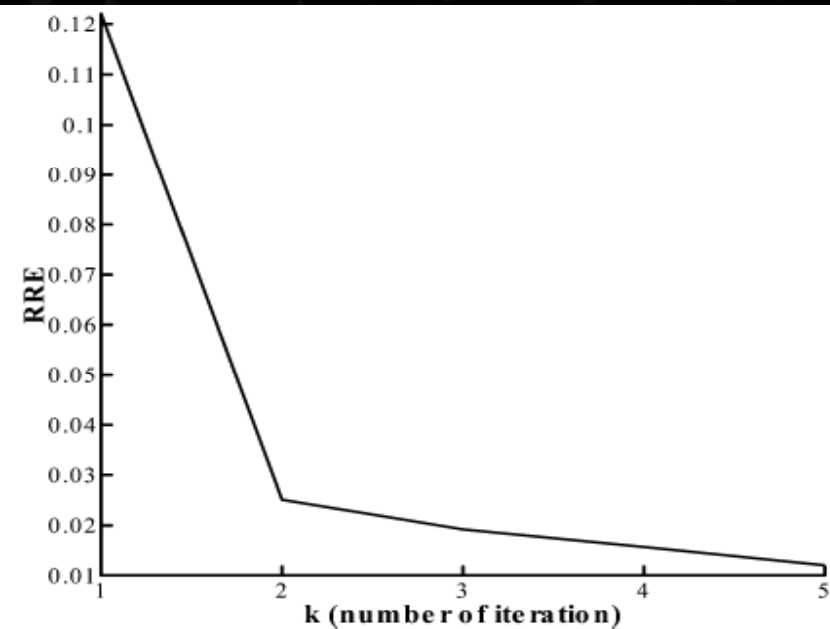


Fig. 9. Plot of  $RRE \equiv \sum_{i=1}^{N_s} |\mathbf{v}_k(\mathbf{r}_i) - \mathbf{v}(\mathbf{r}_i)| / \sum_{i=1}^{N_s} |\mathbf{v}(\mathbf{r}_i)|$ , as a function of the iteration number  $k$ , for the example in Figs. 6–8.

## C. Scalability Study:

- All examples were computed 500MHz P-II computers situated in a networked environment such that the computers may be used for parallel computations.

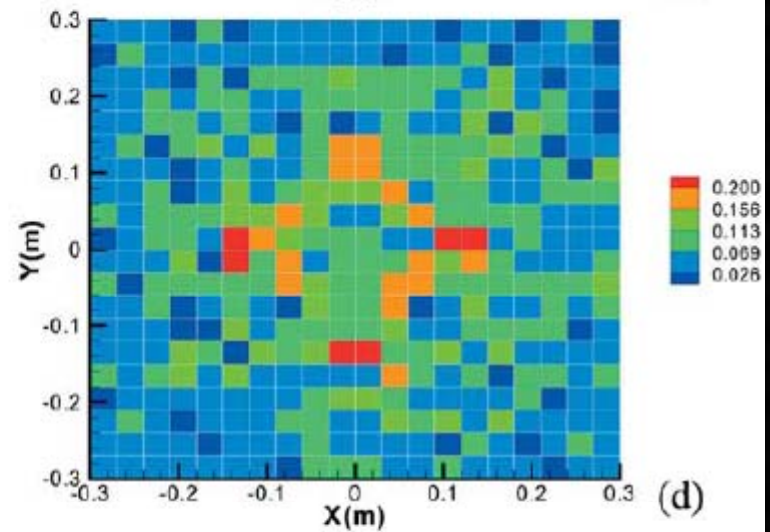
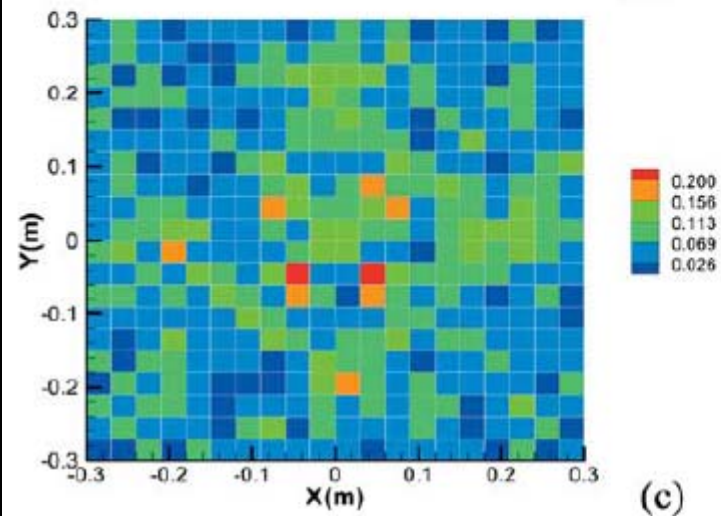
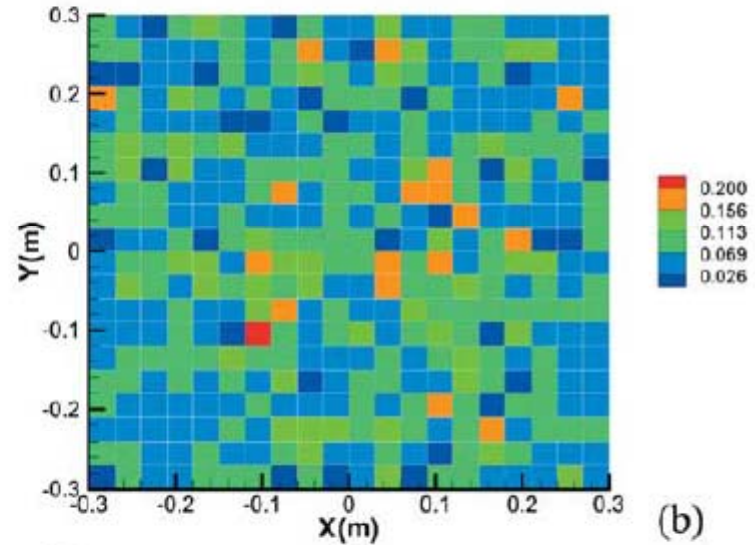
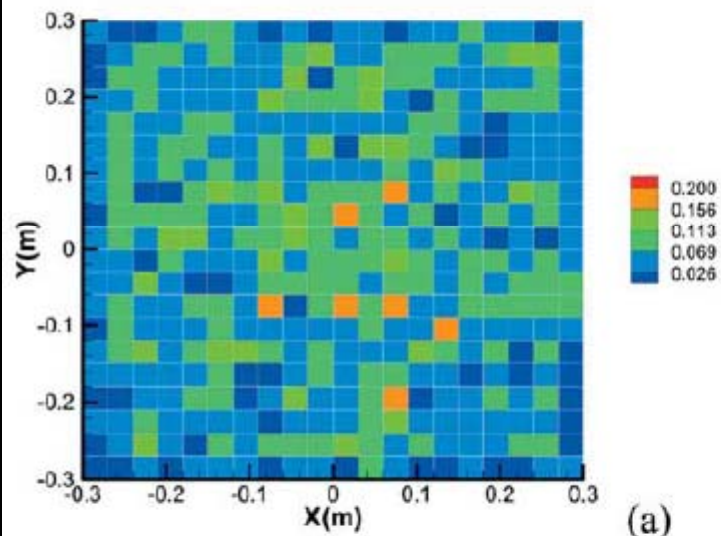
TABLE I  
COMPARISON OF CPU TIMES OF SERIAL AND PARALLEL  
IMPLEMENTATION OF INVERSION ALGORITHM

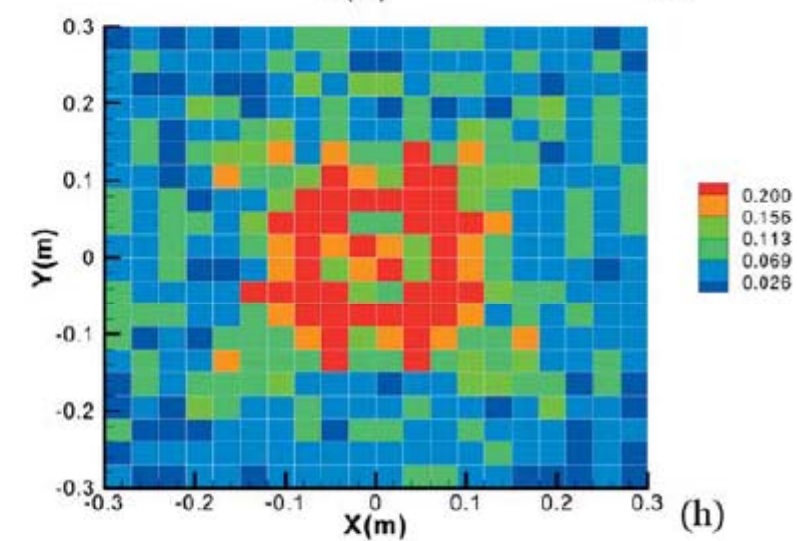
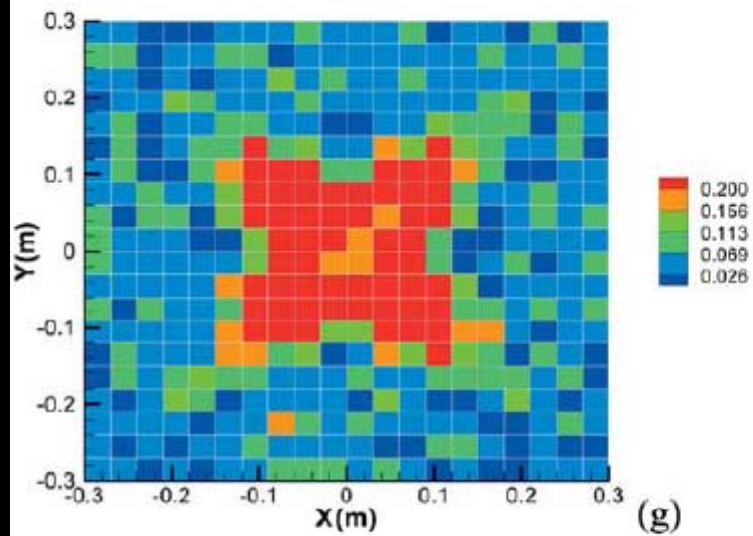
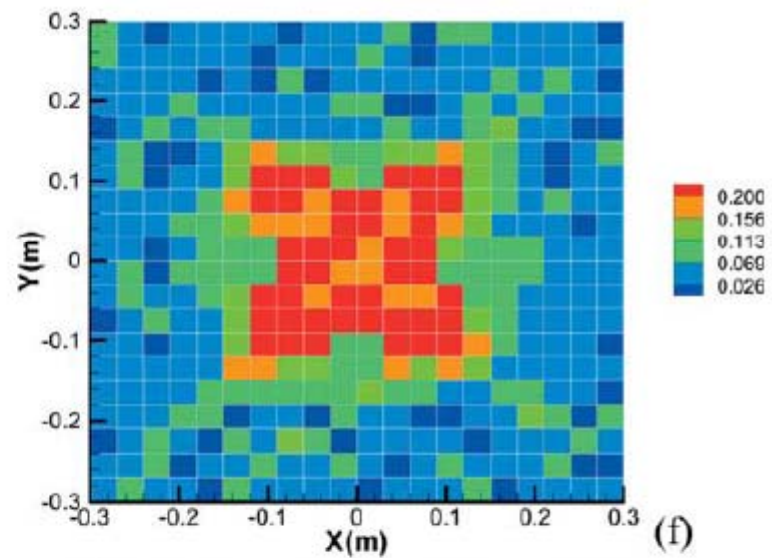
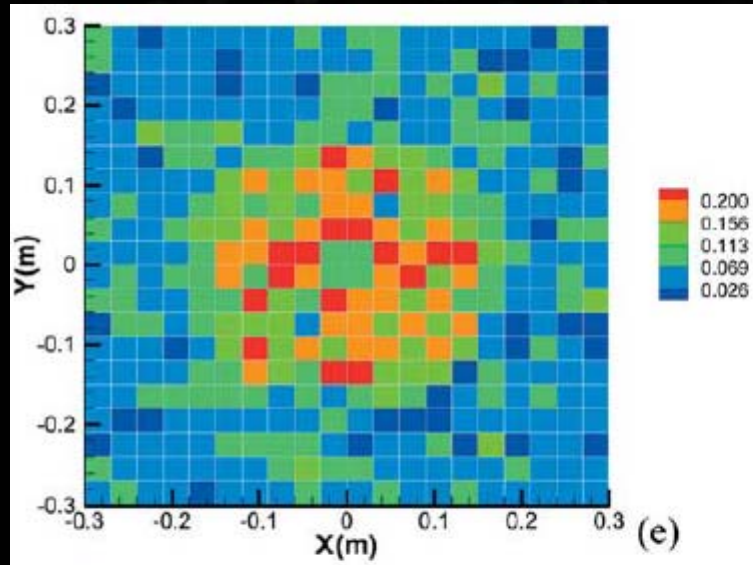
Computation part	Serial code	MPI parallel code		
		8 machines	16 machines	32machines
Measure data	40 min	4 min	2 min	1 min
Table	1885 min	164 min	85 min	43 min
Iteration	135 min	10 min	5 min	2.5 min

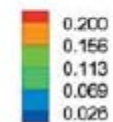
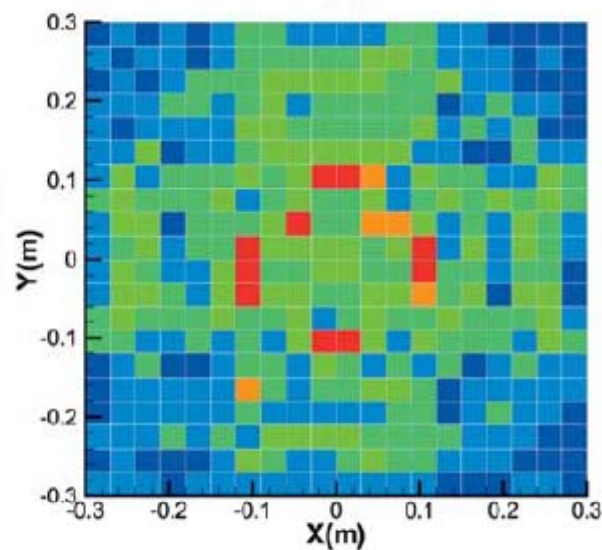
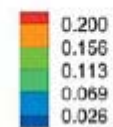
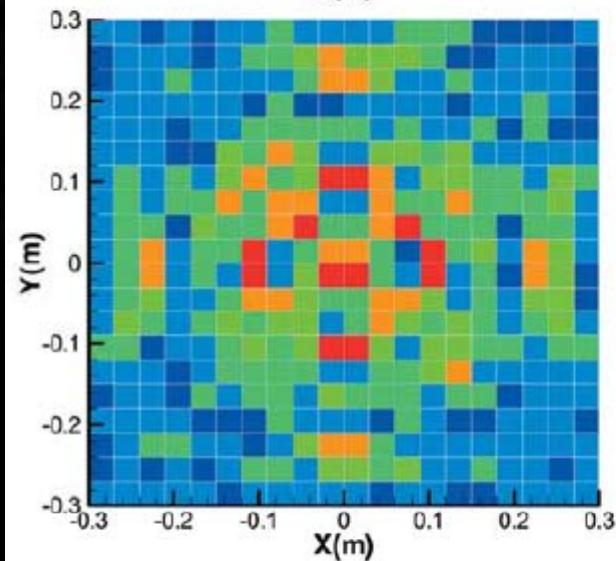
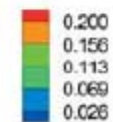
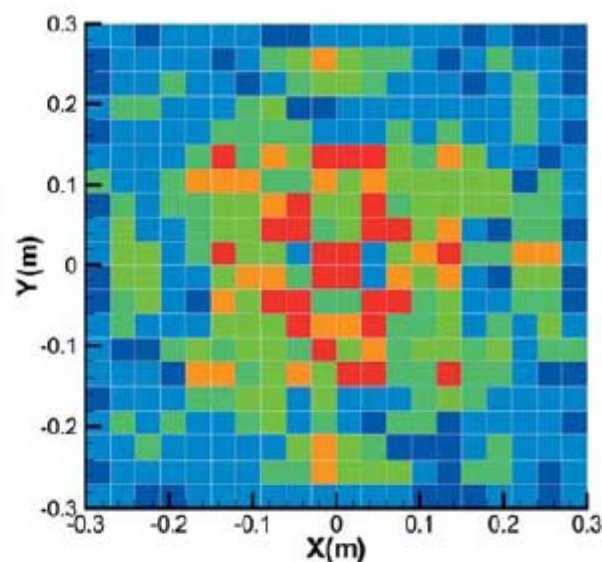
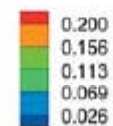
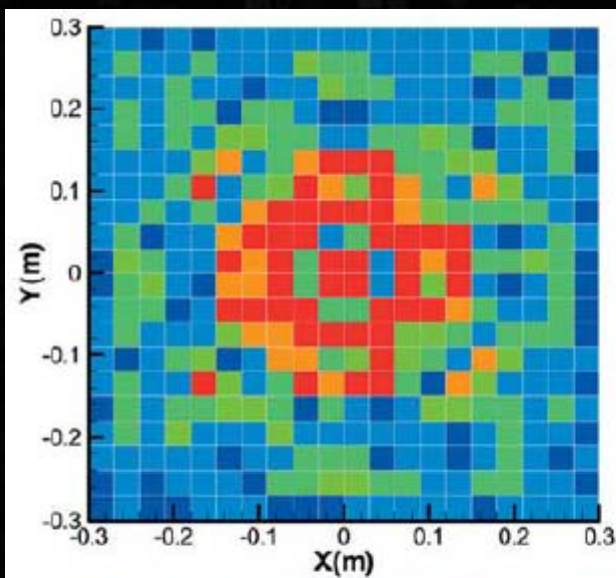
- Such “super-linear” acceleration is likely a consequence of the manner in which the serial and parallel software utilize cache memory, indicating the difficulty in assessing a direct comparison of parallel and serial software

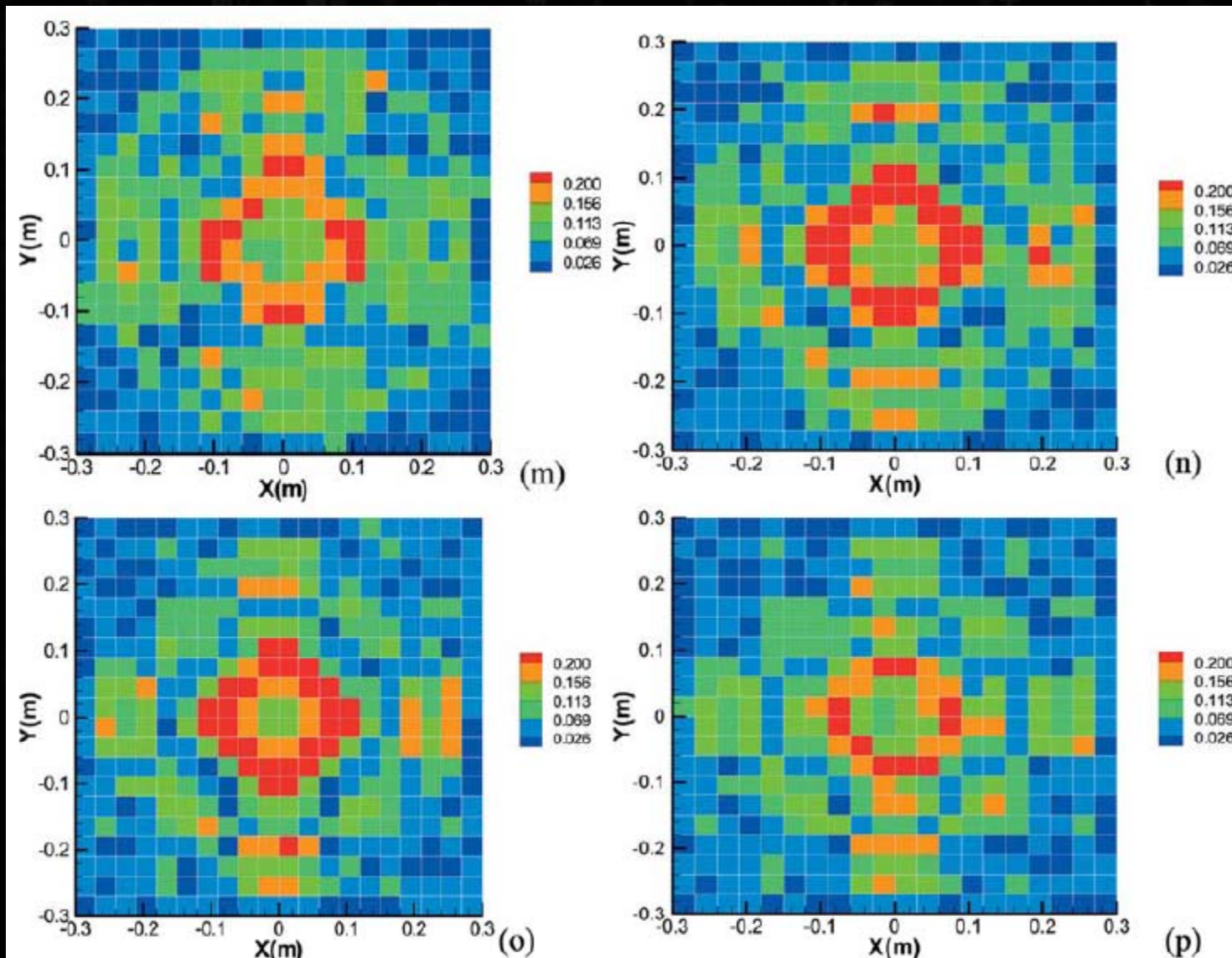
## D. Large Target Dimensions

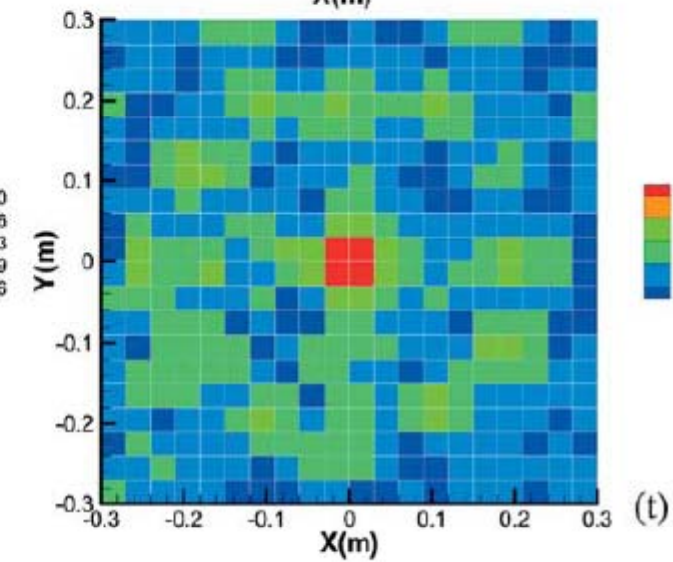
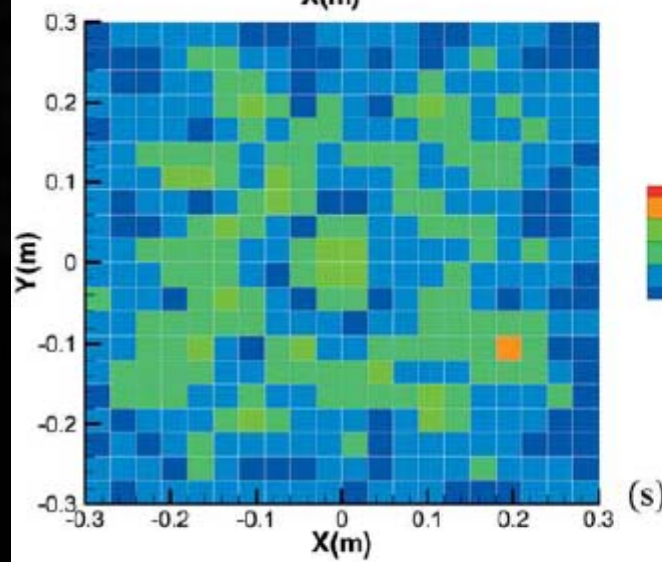
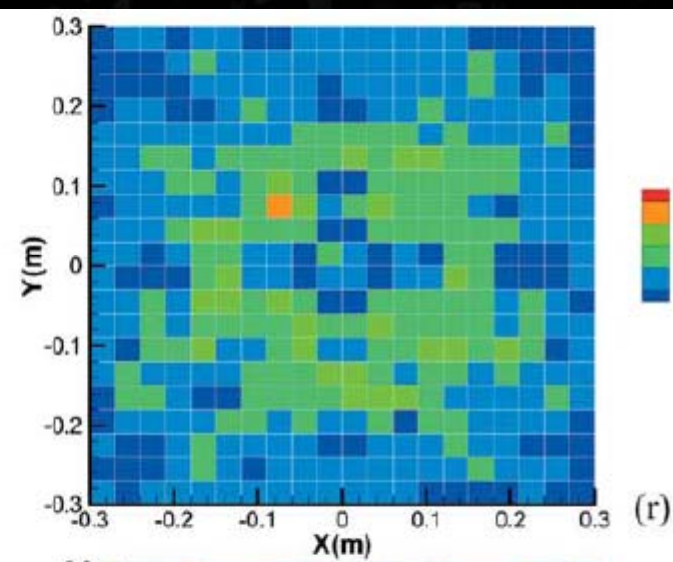
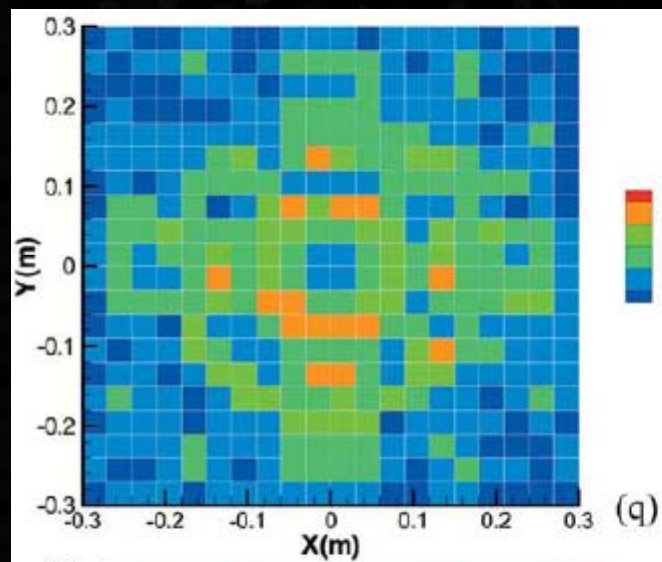
- Inversion quality is typically tied to the target contrast and is also strongly dependent on the target size.
- Using parallel software a  $20 \times 20 \times 20$  computational domain is considered, with the same spatial gridding size as considered in the previous examples.
- The target has a physical size of 30.6 cm x 30.6 cm x 30.6 cm, with target center 35 cm below the interface.
- Within the background soil, at the 500-MHz frequency considered, this corresponds to a buried box of dimension 1.14 wavelengths on a side.
- A Cartesian lattice of  $16 \times 16$  transmitter/receiver coils is placed uniformly in a 1.8 m x 1.8 m domain, centered over the target center, 1 cm above the interface. (So Matrix size for in the iterative Born becomes  $16^4 \times 20^3$ )
- Computation times of approximately 1 h of CPU time per inverse iteration. And made less effective use of cache memory, *vis-à-vis* the smaller problem
- Relative error of 29% is observed for this case.











# Conclusion

- The main focus of this paper was to investigate the feasibility of 3-D inverse scattering for buried dielectric targets, without the use of bore holes.
- Having demonstrated that this may be done relatively accurately, there are several directions for future work like at higher contrasts the accuracy degrades and for larger problems the computational efficiency is an issue. Similarly finding new methods to replace Tikhonov regularization can also be taken into account as a future work.

THANK YOU ...